Journal of Biomedical Materials Research Part A

WILEY

Society For Biomaterials

RESEARCH ARTICLE

Rapid and Inexpensive Image-Guided Grayscale Biomaterial Customization via LCD Printing

Ryan M. Francis[1] | Irina Kopyeva[2] | Nicholas Lai[1] | Shiyu Yang[1] | Jeremy R. Filteau[1] | Xinru Wang[3,4] | David Baker[1,2,3,4,5,6,7] | Cole A. DeForest[1,2,3,4,6,7,8]

[1]Department of Chemical Engineering, University of Washington, Seattle, Washington, USA | [2]Department of Bioengineering, University of Washington, Seattle, Washington, USA | [3]Department of Biochemistry, University of Washington, Seattle, Washington, USA | [4]Institute for Protein Design, University of Washington, Seattle, Washington, USA | [5]Howard Hughes Medical Institute, University of Washington, Seattle, Washington, USA | [6]Institute for Stem Cell & Regenerative Medicine, University of Washington, Seattle, Washington, USA | [7]Molecular Engineering & Sciences Institute, University of Washington, Seattle, Washington, USA | [8]Department of Chemistry, University of Washington, Seattle, Washington, USA

Correspondence: Cole A. DeForest (profcole@uw.edu)

Received: 21 October 2024 | **Revised:** 4 February 2025 | **Accepted:** 4 March 2025

Funding: This work was supported by a Faculty Early Career Development CAREER Award (DMR 1652141, C.A.D.) from the National Science Foundation (NSF) and a seed grant through the NSF-sponsored University of Washington Materials Research Science and Engineering Center (DMR 1719797 to C.A.D.), as well as a Maximizing Investigators' Research Award (R35GM138036 to C.A.D.) and a research grant (R01CA289291 to C.A.D.) from the National Institutes of Health. Graduate student fellowship support was provided by the ITHS (to R.M.F.) and an Interdisciplinary Training Grant (T32CA080416 to I.K.) from the National Institutes of Health. Additional funding was provided by the Howard Hughes Medical Institute (D.B.) and the Audacious Project (D.B., X.W.).

Keywords: 3D printing | additive manufacturing | grayscale | hydrogel | light | photopatterning

ABSTRACT

Hydrogels are an important class of biomaterials that permit cells to be cultured and studied within engineered microenvironments of user-defined physical and chemical properties. Though conventional 3D extrusion and stereolithographic (SLA) printing readily enable homogeneous and multimaterial hydrogels to be formed with specific macroscopic geometries, strategies that further afford spatiotemporal customization of the underlying gel physicochemistry in a non-discrete manner would be profoundly useful toward recapitulating the complexity of native tissue in vitro. Here, we demonstrate that grayscale control over local biomaterial biochemistry and mechanics can be rapidly achieved across large constructs using an inexpensive (~$300) and commercially available liquid crystal display (LCD)-based printer. Template grayscale images are first processed into a "height-extruded" 3D object, which is then printed on a standard LCD printer with an immobile build head. As the local height of the 3D object corresponds to the final light dosage delivered at the corresponding *xy*-coordinate, this method provides a route toward spatially specifying the extent of various dosage-dependent and biomaterial, forming/modifying photochemistries. Demonstrating the utility of this approach, we photopattern the grayscale polymerization of poly(ethylene glycol) (PEG) diacrylate gels, biochemical functionalization of agarose- and PEG-based gels via oxime ligation, and the controlled 2D adhesion and 3D growth of cells in response to a *de novo*-designed α5β1-modulating protein via thiol-norbornene click chemistry. Owing to the method's low cost, simple implementation, and high compatibility with many biomaterial photochemistries, we expect this strategy will prove useful toward fundamental biological studies and functional tissue engineering alike.

1 | Introduction

Global efforts over the past several decades to probe and direct cell biology in vitro have made extensive use of hydrogel biomaterials [1–4]. These water-swollen polymeric networks intrinsically mimic the highly aqueous nature of the body, support cell encapsulation and extended culture, and can be synthetically customized to mimic the physical and chemical aspects of native tissue. Though early successes have capitalized on using homogeneous hydrogels cast in simple mold-defined geometries, recent advances in additive manufacturing have enabled the creation of macroscopically structured gels that span tissue-level scales. While achievable resolutions, fabrication times, costs, and general availability naturally differ between techniques, digital light processing (DLP)-based [5], volumetric [6], extrusion-based [7, 8], filamented light (FLight) biofabrication [9], and open-microfluidic [10] printing now readily permit hydrogel materials to be cast in user-defined geometries. Further, advanced implementation of these methods (e.g., multinozzle extrusion, sequential DLP) can enable the synthesis of discrete multimaterials useful for applications such as exploring geometrically defined co-culture of various cell types and studying tissue interfaces, among others [11, 12].

Despite tremendous advances in additive manufacturing, methods to create non-binary biomaterials with arbitrary and continuously varied physicochemistry remain largely undeveloped. Existing strategies often settle for simple linear or radial gradients that do not necessarily reflect the underlying biology they seek to mimic [13]. As heterogeneous chemical and physical cues underscore virtually all biological signaling events throughout living tissue, techniques that permit user-defined and "grayscale" fabrication/customization of biomaterials are of prime interest. Towards this goal, light-based chemistries offer two particularly distinct advantages: (1) material fabrication is readily controlled in time and space based on when and where light is directed, at potentially high resolutions over large areas, and (2) many photochemistries exhibit predictable dosage-dependence, in that greater photoreaction accompanies longer or brighter light exposures [14–16]. Though the first advantage lies at the core of every light-based printing technology (e.g., DLP, FLight), only a few attempts have exploited that second and uniquely powerful advantage to create grayscale multimaterials [17–20].

Our group recently introduced "grayscale image z-stack-guided multiphoton optical-lithography" (GIZMO), enabling rapid biomaterial photomodulation in full 3D non-binary patterns [19]. While we have demonstrated GIZMO's utility for grayscale physical or chemical modulation of gels at sub-micron resolutions spanning >mm^3 volumes, the technique relies on an in-line acousto-optic modulator capable of controlling the intensity of a femtosecond-pulsed laser throughout raster scanning. As this technique requires specialized expensive equipment (~$500,000) and exhibits fabrication times that scale linearly with construct volume, we sought to develop a complementary method that trades one dimension of spatial control for the ability to be easily implemented with inexpensive and readily accessible commercial instrumentation (~$300) as well as with fabrication times that are fully decoupled from construct size.

Striving to fill this manufacturing niche, we identified liquid crystal display (LCD) screens as the most ubiquitous high-resolution light producers. Consumer resin 3D printers ship with LCD screens designed for radical-initiated photopolymerization and integrated software for specifying pixel illumination patterns. Although LCD printing has gained popularity for its affordability and high resolution, often outclassing far more expensive DLP systems, its applications for tissue engineering are only beginning to be realized. A recent report found that off-the-shelf LCD printers can be used for 3D bioprinting of cell-laden constructs at high resolution (~80 μm) [21]. During normal operation, the printer lowers its stage into a vat of liquid monomer precursor. Beneath this vat, the LCD screen delivers a user-specified light pattern, typically at 405 nm and ~1–10 mW cm^{-2}, confining polymerization to a thin binary-specified layer at the stage. Iteratively retreating the build platform from the LCD screen and projecting a new pattern on a thin monomer layer enables complex 3D structures to be generated in a layer-by-layer fashion. However, if the stage were forced to remain in a fixed position relative to the LCD display, the height of the "to-be-printed" inputted 3D model would correspond to the final light dosage delivered at each *xy*-coordinate. We hypothesized this could provide a route to spatially defining the extent of biomaterial photoreaction.

In this work, we demonstrate that grayscale biomaterial mechanics and biochemistry can be rapidly achieved using an inexpensive and commercially available LCD printer. Here, non-binary image templates are first processed into a "height-extruded" 3D object, whereby input pixel intensity specifies outputted local object height. After slicing the extruded 3D object into a series of cumulative masks, as is typical for LCD 3D printing, the patterns are sequentially projected onto photosensitive gel components to yield the grayscale construct (Figure 1). Notably, pattern geometries are infinitely customizable and are limited only in size by the LCD screen. We demonstrate the utility of this technique by variably patterning the radical chain polymerization of poly(ethylene glycol) (PEG) diacrylate, photomediated oxime ligation-based immobilization of biomolecules within agarose- and PEG-based hydrogels, and a thiol-ene-based tethering of a *de novo*-designed α5β1-modulating miniprotein to control 2D cell attachment and 3D growth within gels. Given the exceptionally low cost, ease of implementation, and broad compatibility with many biomaterial photochemistries, we anticipate this strategy will prove broadly useful towards engineering natively complex tissue constructs at scale.

2 | Materials and Methods

2.1 | Materials

All hydrogel material precursors were purchased from listed commercial suppliers or synthesized as described in the Supporting Information document.

2.2 | Printer Modification and Pattern Generation

All LCD patterning was performed on an Elegoo Mars 4 Ultra resin printer (Table S1). The build platform and resin tank were

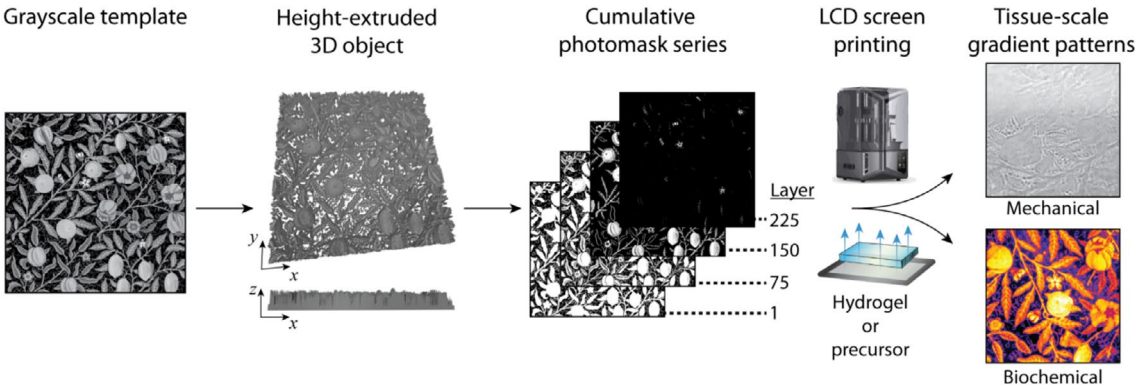

FIGURE 1 | Image-guided grayscale biomaterial customization enabled via LCD printing. A grayscale image template is height-extruded to produce a 3D object with the *z*-dimension representing pixel intensity at a given location. The 3D object is sliced into cumulative photomasks that are sequentially applied to a hydrogel or precursor solution using an LCD printer screen. This gradient patterning technique can be applied to a variety of common photochemical systems, including photopolymerization and biochemical tethering.

removed and replaced with 0.2 mm-thick cover glass treated with Rain-X. Patterning experiments were performed directly on the glass (Figure S1). To minimize overall patterning times, stage motor movements were set to the minimum (0.001 mm). Similarly, motor speed was set to the maximum value to reduce the time between layers.

3D objects were manipulated and sliced in CAD or using the included ChituBox software (Figure S2). 2D images were extruded by converting to .stl objects with a z-dimension equal to the relative intensity of each *x*–*y* pixel (Method S1, Figure S3). The total height of the object was set to 2.55 mm for 8-bit patterning, with layer depth set to 0.01 mm and exposure time set to the maximum desired dosage divided by 255.

2.3 | Photorheometry

A 10 wt.% solution of PEG diacrylate (PEGDA, $M_n \sim 8$ kDa, Sigma Aldrich) containing 5 mM lithium phenyl-2,4,6-trimethylbenzoylphosphinate (LAP; Allevi3D, Philadelphia, PA) was prepared and pipetted in 30 μL droplets onto a custom-built photorheometry plate with a transparent bottom. A 400 nm light source was mounted beneath the plate and set such that the precursor solution was illuminated with 4 mW cm^{-2}. Rheological experiments were performed on an Anton Paar Physica MCR-301 (Graz, AT) with parallel plate geometry at 25°C and 8 mm parallel plate geometry (500 μm gap, 1 Hz, 1% strain). Oscillatory time sweep experiments were performed at constant strain and frequency, collecting measurements every 10 s. The 400 nm light source was turned on for defined intervals and then switched off until mechanical equilibrium was reached before beginning the next dose. Gels were illuminated for up to 17 min, corresponding to a total dosage of 4.08 J cm^{-2}.

2.4 | Fluorescence Recovery After Photobleaching (FRAP)

Precast gels were equilibrated for 24 h in a solution (5 μM) of recombinant Enhanced Green Fluorescent Protein (GFP, MW ~ 31 kDa). FRAP was performed using a Leica SP8X confocal microscope equipped with a 488 nm argon laser and a 25× water immersion objective. Bleaching and imaging scans were performed at 512 × 512 resolution and 5× zoom on the maximum scan speed, resulting in a 0.371 s scan duration. The bleach spot was a circle with a radius of 25 μm. FRAP measurements were performed using 10 bleaching scans (3.71 s) followed by 162 recovery scans (60.10 s). Recovery data in the circular bleach spot can be fitted to a closed-form solution of the simplified diffusion equation using modified Bessel functions [22]:

$$\mathrm{frap}(t) = e^{-\tau_D/2t}\left[I_0\left(\frac{\tau_D}{2t}\right) + I_1\left(\frac{\tau_D}{2t}\right)\right],$$

$$\tau_D \equiv \frac{w^2}{D_f},$$

where frap (t) is the time-dependent fluorescence value in the bleach spot, and w is the spot radius to yield the diffusion coefficient D_f for each gel. A decay curve relating G' and D_f from identically formed hydrogels within the observed dynamic range ($G' = 0.5$ to 10 kPa) was derived as:

$$G' = 34.22e^{-0.12D_f}.$$

2.5 | Using FRAP to Map Spatial Heterogeneity

A simple 14 × 14 pixelated ghost pattern was selected for spatial mapping to minimize the number and complexity of FRAP measurements needed to probe its mechanical properties. FRAP data was collected in a regular grid pattern at about 50 μm depth below the gel surface. The resulting curves were fit to calculate D_f, then interpolated to calculate G' at each location. The resulting values were arranged in a heatmap to compare pattern fidelity with D_f at the bleaching location taken as a proxy for the surrounding 300 × 300 μm pixels. It is important to note the limitations of this assumption considering chain growth hydrogels are known to have naturally high spatial heterogeneity compared to more homogenous step growth counterparts. Additionally, while D_f and G' are certainly related, they are not independent of other factors including solute shape and mesh radius [23].

2.6 | Photomediated Oxime Patterning in PEGDA Hydrogels

A 5 wt.% solution of PEGDA (M_n ~ 575 Da, Sigma Aldrich) was prepared containing $[Ru(bpy)_3]Cl_2$ (200 μM, Sigma Aldrich), ammonium persulfate (2 mM), and DCMAC-NO-MA probe (100 μM, Methods S2–S3, Figure S4, and Table S2). The precursor solution was pipetted between two Rain-X-treated glass coverslips separated by a 0.5 mm-thick silicone gasket before being polymerized under 455 nm light—a wavelength that does not perturb the DCMAC cage [24]. The resulting hydrogel was washed in water for 1 h to remove the photoinitiator, then transferred to the LCD printer and patterned using 405 nm light. The patterned gel was washed overnight in 1 μM AlexaFluor-488 aldehyde (AlexaFluor-488-CHO; XFD488 aldehyde, AAT BioQuest, Pleasanton, CA) or AlexaFluor-594 aldehyde (AlexaFluor-488-CHO [25]) with 0.1% aniline, then for 1 h in water. Patterns were imaged using a Leica Stellaris 5 confocal microscope.

2.7 | Photomediated Oxime Patterning in Agarose Hydrogels

A solution containing 1% ultra-low melting point agarose and 0.5% DCMAC-NO-modified agarose (Methods S4 and S5) was prepared by heating to 80°C and then pipetted between two Rain-X-treated glass coverslips separated by a silicone gasket (width = 0.5 or 1.0 mm). The gel was equilibrated in water for 1 h, then patterned, stained, and fluorescently imaged as with the PEGDA gels described above.

2.8 | Pattern Fidelity Comparison

Template and confocal pattern images were cropped and aligned using Adobe Illustrator, then pixel intensities adjusted using ImageJ to maximize dynamic range without excess saturation and to equalize the number of pixels in each image. Using a custom Python script described previously [19], a random subset of the pixel locations from the template was sampled such that each of 64 bins (each containing 4 sequential 8-bit values) contained an approximately equal population. Each pixel location was plotted on a heatmap with x and y axes representing the template and pattern intensity, respectively. An identical pattern and template will result in all points falling on the $x=y$ parity line. Additionally, a subtraction plot was generated by simply subtracting the pixel intensities in the template from those in the pattern.

2.9 | hMSC Encapsulation and Patterning of NeoNectin^{E44C}

Human mesenchymal stem cells (hMSCs) were purchased from RoosterBio Inc. (Frederick, MD) and cultured in Mesenchymal Stem Cell Growth Medium 2 (PromoCell GmbH; Heidelberg, Germany) supplemented with 1× Penicillin–Streptomycin (PS) in a standard 37°C, 5% CO_2 cell culture incubator. Cells were passaged 1:10 upon reaching 80% confluency. All experiments were conducted with cells at passage 5.

For encapsulation, thiol-ene gels were formed off stoichiometry with monomers and gel precursors combined at 3 mM 8-arm PEG-norbornene (PEG-NB; JenKem; Plano, TX), 10 mM dicysteine peptide crosslinker (Ac-GCRDLPESGGPQGIWGQDRCG-NH_2) (GenScript, Piscataway, NJ), and 5 mM LAP to preserve additional norbornene sites for modification with a carboxyfluorescein-modified NeoNectin^{E44C} (FAM-NeoNectin^{E44C}, Method S6). hMSCs were encapsulated within gels at a density of 2×10^6 cells mL^{-1}; upon mixing, 35 μL droplets were pipetted between Rain-X-coated glass coverslips spaced at 500 μm. The precursor solution with suspended cells was polymerized by exposure to 405 nm light on the LCD printer screen for 1 min. Immediately following this, cell-laden gels were soaked in the FAM-NeoNectin^{E44C} solution (200 μM) with LAP (5 mM) for 1 h at 37°C, then patterned on the printer for 70 s. Following this, the gels were washed 3×30 min in clean media to remove excess protein. The gels were cultured for 7 days and then fixed with 4% paraformaldehyde for 1 h, after which they were washed 3×10 min in tris-buffered saline (TBS) and permeabilized with 0.5% Triton X-100 solution in TBS. The actin cytoskeleton and nuclei were subsequently labeled with 1:500 AlexaFluor-532-Phalloidin (Thermo Fisher) and 1:1000 4′,6-diamidino-2-phenylindole (DAPI), respectively, in TBS. The gels were then rinsed in TBS and imaged on a Leica Stellaris confocal microscope. Cell eccentricity was analyzed with Cell Profiler 4.0 [26].

2.10 | Statistical Analysis

Data analysis was performed in GraphPad Prism. Values are expressed as mean ± SD (95% CI).

3 | Results

3.1 | Modification of a Resin Printer for Gradient Patterning

During conventional operation of an LCD-based 3D printer, a to-be-printed 3D input model is first sliced into a stack of regular z intervals of defined thickness. The LCD screen then delivers a sequence of binary pixel illumination patterns, each defining which xy-positions will be polymerized at a z-location specified by the build plate. To achieve grayscale fabrication, we sought to repurpose such illumination sequences to ultimately specify the light dosage delivered at each xy position on an immobile sample. Here, stationary fabrication (i.e., the build plate does not move in z throughout illumination) results in the delivery of more light repetitions to "taller" regions of the input model. For example, a conical 3D input model would print as a circle with a dosage exposure that decays radially. In doing so, we effectively re-encode z-dimensional information from the input model into light dosage (and thus reaction extent) in the grayscale print.

We initially implemented this strategy using an Elegoo Mars 4 Ultra resin printer ($278 at time of purchase in October 2023, $209 at the time of manuscript submission in October 2024), repurposing its 7-inch 9 K mono LCD screen. Here, we removed the build platform and minimized print delays between "layers" (usually reserved to accommodate platform movement). This delay can be lengthened if printing with temperature-sensitive

samples, allowing heat dissipation to occur between rounds of light exposure. The Mars 4 Ultra's 405 nm LCD screen intensity was measured at $4 \pm 0.1\,\mathrm{mW\,cm^{-2}}$, consistent across the entire screen. Printing through the stock basin with perfluoroalkoxy (PFA) base—typically employed to prevent polymerization at the basin surface—was possible, though light scattering and attenuation necessitated longer fabrication times and yielded poorer print resolutions. Alternatively, we found that removing the PFA base and simply placing a cover glass layer directly on the LCD screen resulted in dramatically improved grayscale processing: in addition to patterning speed improvements by decreasing attenuation, better refractive index matching minimized scattering.

For each non-binary print, we performed a height extrusion on a grayscale input image. The total pattern height and layer depth settings were configured to give the desired range of grayscale values (Figure 1). For example, an 8-bit image (255 nonzero values) can be encoded using a 2.55 mm "z maximum" with an individual layer thickness of 0.01 mm (Figure S3). Dwell time per layer is then calculated as the maximum exposure time divided by the number of layers. If the photokinetic properties of the material are well characterized, we anticipate that it would be possible to recreate the original input with high fidelity, even if it contained complex features and gradients.

Since the aim of this study is to repurpose an inexpensive and commercially available LCD printer for grayscale fabrication, it is vital that the LCD light dosage and wavelength are compatible with established photochemistries. For radical-initiated hydrogel polymerization, the popular type I photoinitiator LAP is extremely sensitive to 405 nm light and amenable to tissue engineering activities such as cell encapsulation [27]. Direct photocaging and radical-free processes are slightly more challenging and often have synthetic prerequisites, but there is a growing selection of redshifted and synthetically accessible options. For example, the dicarboxymethylamino coumarin cage (DCMAC) [28, 29] has proven extremely sensitive in our hands both to multiphoton and near-UV/blue light single-photon activation [19]. For traditional caging groups such as *ortho*-nitrobenzyl that have poor sensitivity to 405 nm light, there are many affordable stereolithographic (SLA) printing solutions available with alternative specifications, including blue-shifted light sources (e.g., 365–385 nm) and higher screen intensities that could be similarly modified. As a result, this technique should allow complex gradient patterning both in physicochemical systems such as gel photopolymerizations and in biochemical patterning through the selective immobilization of biomolecules (Figure 1).

3.2 | Grayscale Patterned Gel Photopolymerization

Chain growth polymerizations are already exploited with high frequency in stereolithographic 3D printing. Most commercial resins contain a mix of acrylate- or acrylamide-containing monomers alongside a photoinitiator. Hydrogel fabrication via chain growth acryl chemistries is identical, but with precursors that are explicitly water soluble and able to form a hydrated network. Acrylated polymer chains, including poly(ethylene glycol) (PEG) or structural biomolecules such as gelatin and hyaluronic acid, have been used to fabricate hydrogels for a variety of biological applications. In radical chain growth polymerization, the light-exposed photoinitiator generates an active radical that propagates through unsaturated carbon–carbon bonds on the monomer to yield high molecular weight chains (Figure 2A). Since one active radical will yield many propagation events, photoinitiators with small molar extinction coefficients (e.g., LAP ~$50\,\mathrm{M^{-1}\,cm^{-1}}$ at 405 nm) can be used at low and cytocompatible concentrations. Even so, the radical propagation process is known to be dose-dependent due to spontaneous termination events, including radical decay through reactions with abundant oxygen in the aqueous precursor solution. We hypothesized that the modified LCD printing strategy could be applied to form complex mechanical gradients via grayscale photopolymerization.

To investigate the dose-dependent evolution of gel mechanics, we performed photorheological measurements of 10 wt.% PEG diacrylate (PEGDA) (M_n ~ 8 kDa) hydrogels after periodic doses of 400 nm light. This experiment yielded gels with tunable compressive moduli (G') from 0.4 to 10 kPa, spanning nearly two orders of magnitude (Figure 2B). To further investigate the variably polymerized networks, we quantified protein diffusion in each using fluorescence recovery after photobleaching (FRAP). Here, formed gels were equilibrated with enhanced green fluorescent protein (GFP, 31 kDa). FRAP measurements were performed using a confocal microscope, and diffusion coefficients (D_f) were determined for gels with varied but known degrees of polymerization. Relating these two datasets yielded a correlation between compressive modulus and protein diffusivity for this specific gel system that was used to infer spatial variations in stiffness inside patterned hydrogels (Figures 2C and S5).

A grayscale pattern in the shape of a pixelated cartoon ghost was prepared to test gradient photopolymerization using the LCD printer. Four unique grayscale values were assigned to different parts of the pattern before height extrusion and fabrication (Figure 2D–F). The resulting pattern was partially visible to the naked eye, a feature we have previously observed in hydrogels with heterogeneous stiffness [30]. This is likely due to slight differences in refractive index and swelling ratio between soft and stiff regions.

To quantify and map the spatially heterogeneous mechanical properties, we collected FRAP measurements in a regular grid pattern across the x–y plane and calculated local D_f values for each region. Since the chosen pattern was uniform across its 14×14 "pixels" (not including the high-intensity protective border), each FRAP measurement was taken as a proxy for the diffusivity throughout the corresponding ~$300 \times 300\,\mu\mathrm{m}$ square "pixel". Softer regions of the pattern (e.g., whites of eyes) that received less light dosage show markedly faster fluorescence recovery than higher dosed and stiff regions (e.g., pupils) (Figure 2G). Importantly, it was also possible to achieve intermediate stiffnesses across a range of values corresponding to the inputted height map. By applying these diffusivity measurements to the previously generated fit, we could infer local G' values throughout the patterned gel. Mapping these values back to their original locations yields a spatial map of local mechanical values that closely resembles the input image (Figures 2H and S6). Gradient photopolymerization performed in this way allows the fabrication of heterogeneous materials with rapid spatial mechanical changes on the order of ~100 μm (Figure S7).

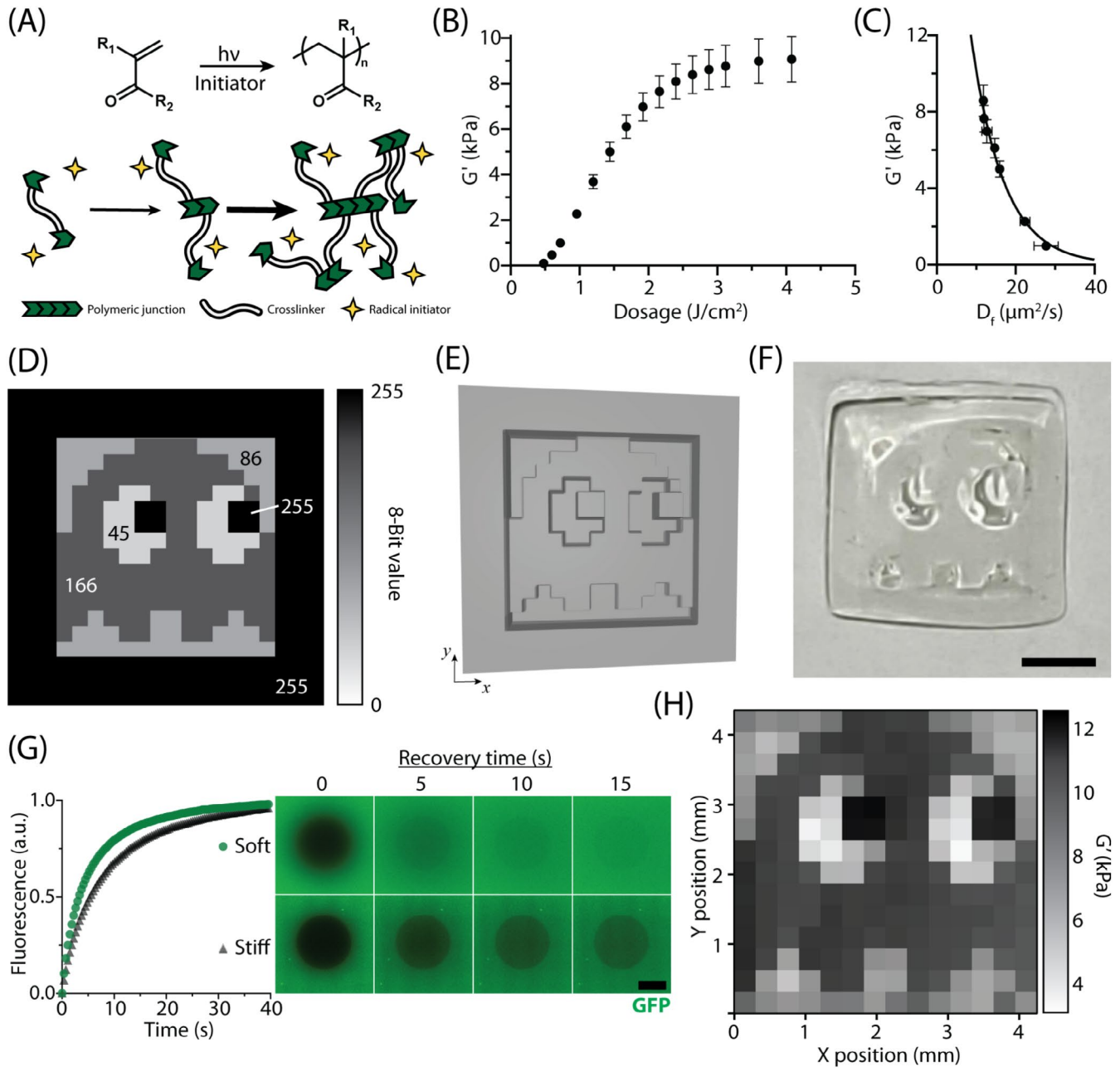

FIGURE 2 | Grayscale stiffening of PEGDA-based hydrogels. (A) Chemical and cartoon depictions of acryl-based chain growth polymerization. Cartoon adapted with permission from ref[2]. R_1 = H, CH_3; R_2 can represent many chemistries. (B) Varied 400 nm light dosage yields gels with compressive moduli spanning nearly 2 orders of magnitude in a 10 wt.% 8 kDa PEGDA hydrogel. Values are expressed as mean ± SD, $n = 3$. (C) FRAP data matched with known compressive moduli is used to derive a relationship between compressive modulus and diffusion coefficient for a 31 kDa fluorescent protein in 10 wt. % 8 kDa PEGDA hydrogel. (D) 2D height map of an arbitrary pattern with annotated 8-bit pixel intensities (inverted). A high-intensity border is included to protect mechanical integrity during downstream processing but is not necessary. (E) Height extrusion from the grayscale image template shown in panel D. (F) A gel photopolymerized according to the grayscale pattern in panels D–E. The pattern is slightly visible due to refractive index changes at mechanical borders. Scale bar = 2 mm. Total fabrication time = 10 min. (G) Representative FRAP curves and timestamped images from a soft (top, whites of eyes) and stiff (bottom, pupils) region of the hydrogel in panel F. Scale bar = 25 μm. (H) Spatially mapped compressive moduli for the hydrogel in panel F inferred from FRAP-derived calculations of diffusivity.

3.3 | High-Resolution, Large-Scale Patterned Biomolecule Immobilization

In addition to radical-mediated hydrogel photopolymerization, we hypothesized that the LCD printer screen could deliver enough light to drive radical-free uncaging reactions, including that for photomediated oxime ligation-based immobilization of biochemical cues within preformed hydrogels. Towards this goal, we turned to the use of dicarboxymethyl aminocoumarin-caged oxyamines (DCMAC-NO), demonstrated previously to exhibit high light sensitivity and semi-linear dose dependence below the saturation dose. To

introduce this photocaged reactive handle within gels formed via radical chain polymerization, we synthesized and characterized a novel methacrylate-modified variant of this species (DCMAC-NO-MA).

The photomediated oxime reaction proceeds through light-induced cleavage of the carbamate linking group followed by covalent ligation of an aldehyde-tagged payload to form a stable oxime bond (Figure 3A). After photolysis, the reaction proceeds spontaneously but exhibits significantly enhanced kinetics in the presence of benzenamine catalysts (e.g., aniline, 4-amino-L-phenylalanine) [31]. Gels were precast with a known concentration of the DCMAC-NO-MA probe, photopatterned via grayscale LCD exposure, followed by incubation with the aldehyde-labeled payload (in this case a fluorophore) and catalyst. Following diffuse removal of any unbound dye, the selectively immobilized dye was visualized via confocal microscopy (Figure 3B). As expected, patterning resolution was enhanced when the PFA membrane was removed (Figure S8).

To determine the optimal 405 nm dosage for a linear patterning response in DCMAC-NO-decorated hydrogels, we exposed the small molecule to variable light doses and quantified the relative extent of uncaging via liquid chromatography–mass spectrometry (LC–MS). Here, peaks corresponding to the emergence of the uncaged DCMAC alcohol byproduct were integrated for kinetic quantification (Figure 3C, Methods S7 and S8). The relationship between 405 nm light dosage and reaction extent can be approximated as a pseudo first-order reaction with $k = 1.2 \pm 0.2\,\mathrm{cm}/^2\mathrm{J}^{-1}$ and a reaction half-life of $0.6 \pm 0.1\,\mathrm{J/cm}^{-2}$, corresponding to 2.5 min of irradiation at $4\,\mathrm{mW/cm}^{-2}$ (Figure 3D). To validate the utility of these constants in hydrogel photopatterning, a process that is abstracted by several steps from decaging in solution, we exposed DCMAC-NO-modified hydrogels to linear dosage gradients with varying endpoints prior to oxime-based immobilization and quantification of a fluorescent aldehyde dye. Here, a series of square wedge patterns with height ratios 1:2:3 were patterned into the gel using print settings corresponding to 3, 6, and 9 min of total exposure (i.e., 0.72, 1.44, and $2.16\,\mathrm{J\,cm}^{-2}$, respectively). Height-mapping these wedges was expected to result in a linear dosage gradient across the y-dimension and constant dosage across x. After staining with AlexaFluor-488-CHO, relative fluorescence was compared between the curves, revealing near-identical dose-dependent responses, but which were slightly below and more linear than that of the photocaged probe in solution (Figures 3E and S9). This is potentially attributable to small amounts of attenuation from scattering or incomplete ligation of the fluorophore, though these results are advantageous for gradient patterning.

In addition to dose response, we next evaluated the LCD screen's resolution limit for biochemical patterning. According to Elegoo documentation, the illumination pixel size in the Mars 4 Ultra is $18 \times 18\,\mu\mathrm{m}$, but some spreading of the non-collimated light is expected, particularly as it passes through samples that are far thicker than the recommended layer depth for resin printing. A series of lines of known width ranging from 20 to 500 μm were patterned into DCMAC-NO-modified agarose hydrogels using the LCD screen. Agarose was employed due to its negligible swelling, helping ensure accurate comparison of post-staining lines with the template. The largest lines (150–500 μm in width) were reproduced with high fidelity but showed some widening (typically 20–40 μm) at the edges, presumably due to the spreading of uncollimated light. The smaller lines showed significant deviation from the template dimensions as well as reduced maximum intensity, although peaks with full width half maximum (FWHM) as small as 100 μm were achieved (Figures 3F and S10). These results are in agreement with observed resolution limits in DLP-patterned biomaterials where the minimum resolvable features are often somewhat larger than the theoretical minimum dictated by pixel size [32]. Scattering and attenuation also place limits on the maximum pattern thickness achievable by this technique. In PEG-based hydrogels, we routinely observed some decrease in pattern intensity with depth, but patterns remained visible and sharp beyond 1 mm (Figure S11). Finally, the DCMAC-NO-acryl probe was used to pattern a 1:1 grayscale reproduction of SOX10 expression from a murine melanoma section [33] into a precast PEGDA hydrogel, demonstrating the ease with which biological geometries can be incorporated into this image-guided workflow (Figure 3G).

With a solid understanding of the dose-dependent response and minimum feature size in this system, we set out to demonstrate the advantages of patterning using a large LCD screen. Namely, fabrication time is independent of pattern size provided the sample is smaller than the screen itself. Here, we cast a large DCMAC-NO-modified agarose gel (5 cm diameter) and patterned it with a large grayscale reproduction of William Morris' "Pomegranate" (Figure 4A). Subsequent staining with aldehyde-tagged AlexaFluor-594 revealed a faithful representation of the pattern with clearly differentiated grayscale values between the background and brightest sections of the image. For example, leaves are clearly visible against a dark background with brighter vein structures running between (Figure 4B,C), while flowers show a clear intensity gradient from petals to receptacle (Figure 4C, bottom). We next assessed the pattern fidelity by aligning excerpts from the template and pattern images pixel-by-pixel and comparing their respective intensities (Figure 4D). From the aligned images, a binned sample of pixels was collected to represent regions across the 8-bit intensity range. These comparisons were plotted as a parity heatmap with points on $y = x$ corresponding to a perfect template-pattern match (Figure 4E). The Morris pattern is faithful to its template image, particularly above pixel intensities of 100. Darker regions tended to be slightly overpatterned, partially due to the nonzero background in confocal microscope images. This becomes obvious if the pattern and template images are subtracted (Figure 4F, blue/green). Additionally, many of the underpatterned pixels (Figure 4F, pink/orange) appear to reside in a damaged portion of the gel. The majority of the patterned regions, however, appeared black (well-matched) in the subtraction plot, as desired. In future applications where the local concentration of a biomolecule tether must be precisely controlled, it should be possible to perform an initial calibration pattern, then refit the template pixel intensities to yield even more faithful patterns.

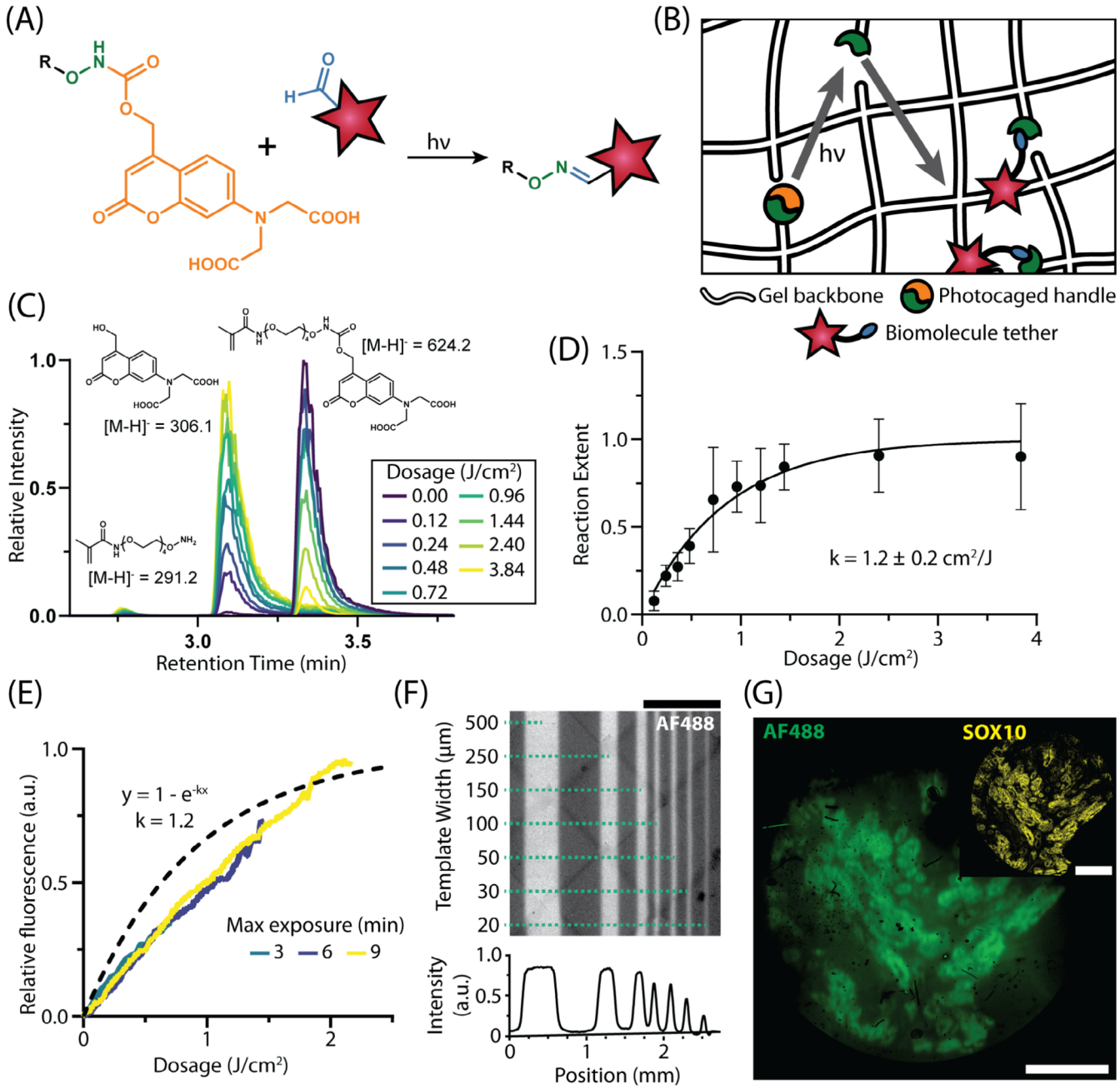

FIGURE 3 | Photomediated oxime ligation enables grayscale biochemical functionalization of gels. (A) A photomediated oxime ligation proceeds through removal of the DCMAC cage (orange), liberating an oxyamine handle (green) prior to covalent ligation with aldehyde-tagged (blue) biomolecule tethers. (B) Photopatterned immobilization of biomolecules proceeds along the hydrogel backbone as the DCMAC photocage cleaves in response to light. (C) Liquid chromatography–mass spectrometry (LC–MS) traces show a light dose-dependent increase of the coumarin-alcohol uncaging product ($[M-H]^- = 306.2$) and liberated oxyamine ($[M-H]^- = 291.2$) and a decrease of the caged DCMAC-NO-MA probe ($[M-H]^- = 624.2$). (D) Quantitative analysis of LC–MS peak area yields the photochemical constant for DCMAC-NO-MA uncaging at 405 nm. Values are expressed as mean ± SD, $n = 3$. (E) AlexaFluor-488-CHO is immobilized in gels following 3 distinct linear light exposure gradients (between 3-, 6-, or 9-min max exposure over 3 mm). When normalized for dosage, response curves match one another and are similar to that determined for in solution DCMAC uncaging (dotted line). (F) Above: LCD-patterned AlexaFluor-488-CHO immobilization in lines of decreasing widths. Below: Average pixel value pixel columns across the upper image. Scale bar = 1 mm. (G) A 1:1 reproduction of SOX10 expression in a murine melanoma section (yellow). The pattern is made from immobilized AlexaFluor-488-CHO (green) in a PEGDA hydrogel. Scale bars = 2 mm.

3.4 | Patterned Integrin-Mediated Cell Attachment Using a De Novo-Designed Protein

Thiolated cargo immobilization can also be photopatterned in grayscale using the LCD printer screen via a radical-mediated thiol-ene conjugation. Many proteins either contain natively reduced cysteine side chains or can be produced recombinantly with a free thiol to enable patterned immobilization of a variety of enzymes and biological cues. Towards patterning cell spreading in 2D and 3D cell culture, we identified a

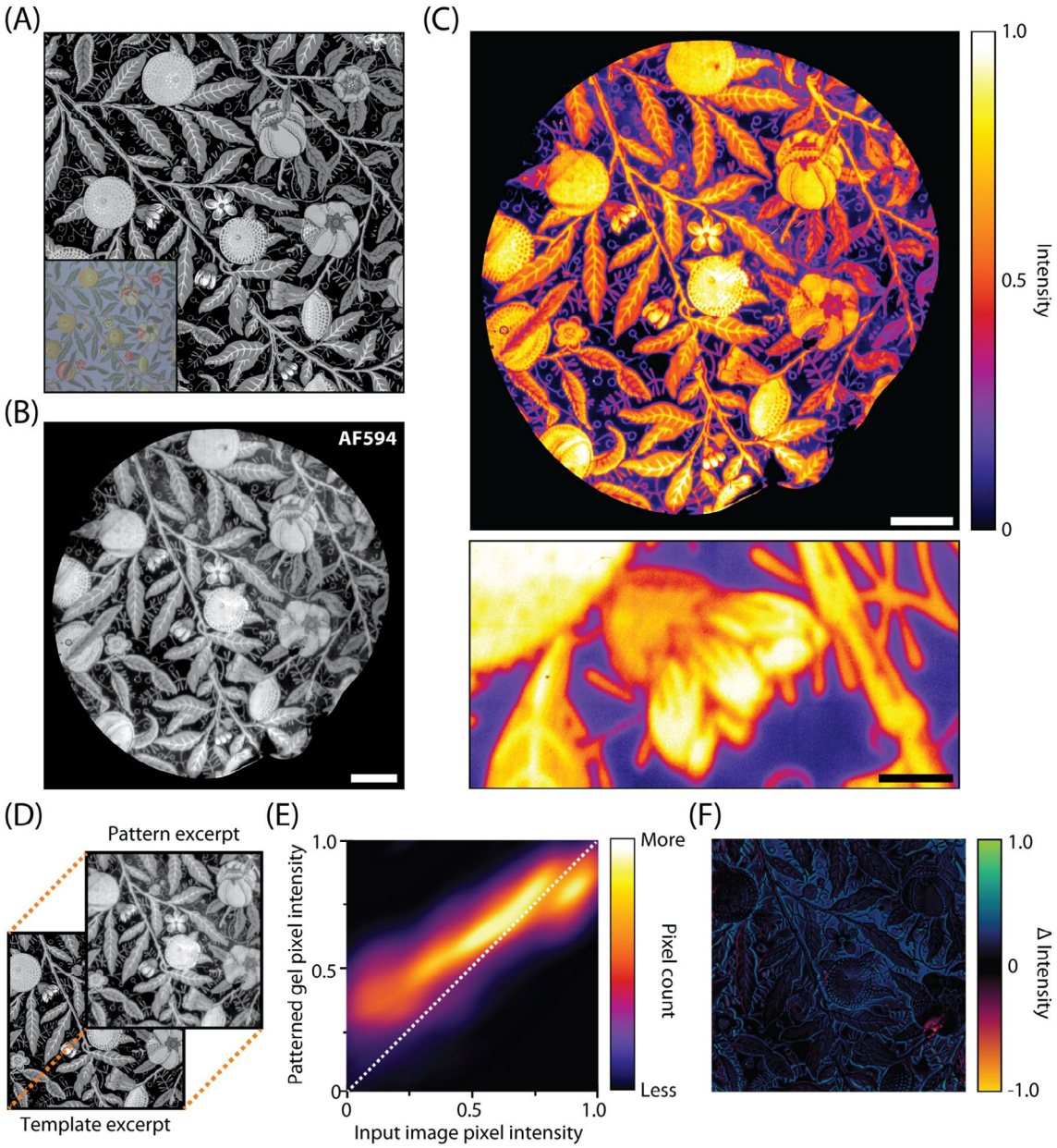

FIGURE 4 | Grayscale image-guided biochemical patterning of agarose gels via photomediated oxime ligation. (A) Grayscale crop of William Morris' "Pomegranate" (1864–5). Inset is the original color drawing. *Source:* The Metropolitan Museum of Art. (B) Patterned AlexaFluor-594-CHO immobilization in a large agarose hydrogel via photomediated oxime ligation. A 500 μm maximum intensity projection. Scale bar = 5 mm. (C) A "sequential colormap" of the patterned gel in panel B reveals the range of gradient immobilization, with a magnified subset shown below. Scale bars = 5 mm (top), 1 mm (bottom). (D) Excerpts from the template and pattern are sized and aligned prior to pixel-by-pixel comparison. (E) Parity heatmap of the floral-patterned gel. Points above the parity line are too intense or over-patterned while points below are under-patterned. The trend at lower pixel intensities is expected due to the non-zero background of confocal images. (F) Pixel-by-pixel subtraction of the aligned pattern and template images reveals regions of under- (pink/orange) and overdosed (blue/green) light during patterning. Minimal color throughout further highlights good overall patterning fidelity.

recently reported and *de novo*-designed α5β1 integrin binder [34]—NeoNectin—for thiol-ene patterning. Here, we employed a variant of this protein engineered to contain just a single cysteine residue installed at a solvent-accessible location (NeoNectin^{E44C}), thereby permitting site-specific tethering of the bioactive protein to ene-containing hydrogels (Figure 5A) [35]. Human mesenchymal stem cells (hMSCs) were either encapsulated in or surface-seeded on a PEG-peptide hydrogel formed via step polymerization of a dicysteine-containing matrix metalloproteinases (MMP)-degradable peptide and an 8-arm PEG norbornene. Gels were polymerized with LAP photoinitiation on the LCD screen (exposure time 1 min) with a stoichiometric excess of norbornene functional groups prior to incubation with a fluorescently tagged NeoNectin^{E44C} and LAP photoinitiator. At this point, a second round of LCD-based photopatterning was performed to selectively immobilize NeoNectin^{E44C} in a variably wide stripe pattern across the gel (Figure 5B). After 7 days of incubation, surface-seeded cells were fluorescently labeled to reveal marked cell spreading and attachment only in regions containing immobilized

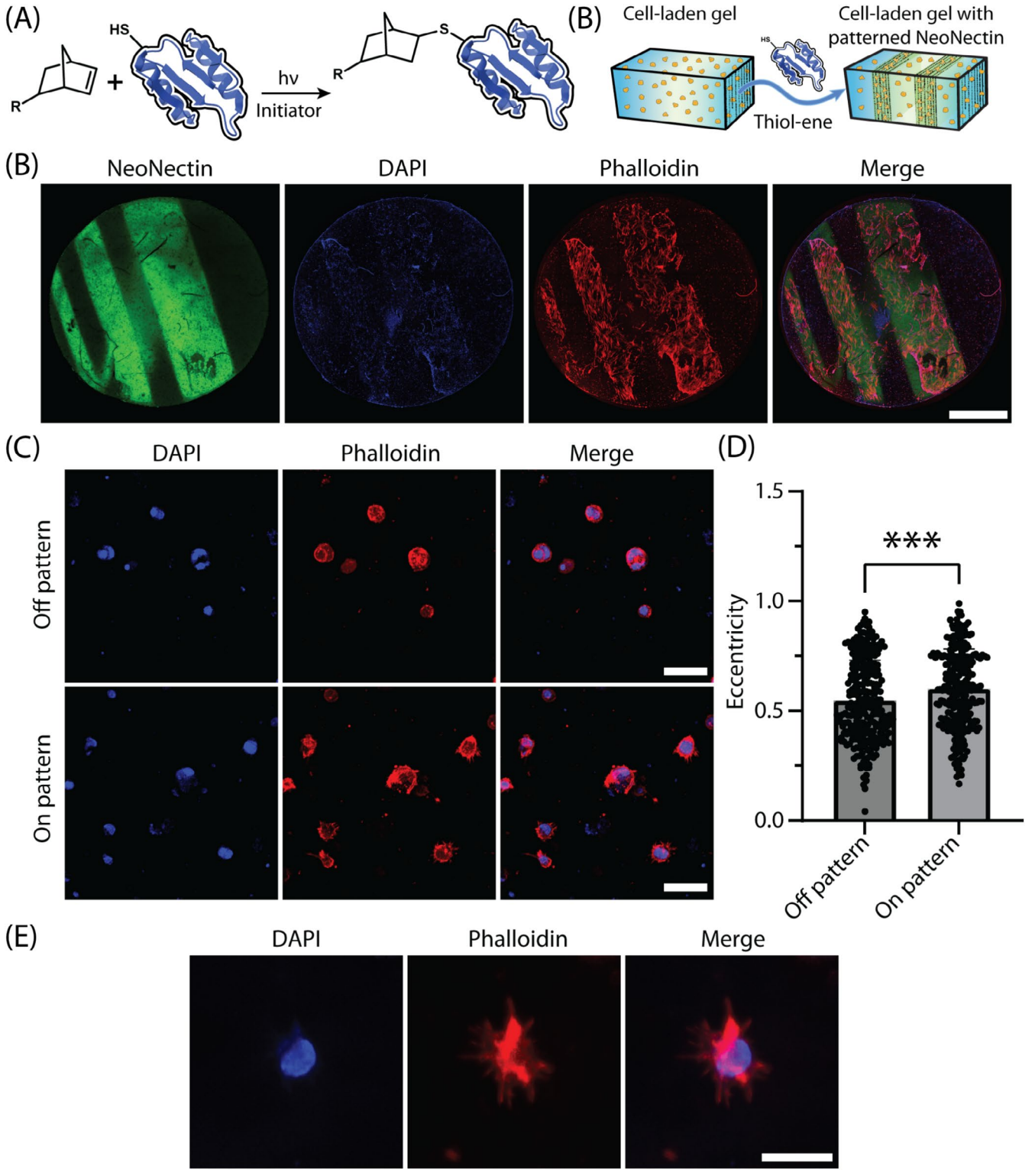

FIGURE 5 | Thiol-ene-patterned NeoNectin selectively drives hMSC attachment and spreading on and within synthetic PEG-peptide gels. (A) Protein immobilization in a thiol-ene PEG-peptide hydrogel proceeds through radical-mediated ligation of the thiol side chain of the protein's sole cysteine residue with excess norbornene groups on the hydrogel backbone. (B) Cells respond to the photopatterned NeoNectin pattern. (C) Confocal imaging of the hMSCs seeded onto hydrogel surfaces containing a stripe pattern of immobilized FAM-NeoNectin^{E44C} (green). Image taken after 7 days of culture with immobilized protein. Nuclei are stained in blue, Actin cytoskeleton in red. Scale bar = 2 mm. (D) Representative images of hMSCs encapsulated in a thiol-ene hydrogel taken 7 days after patterned immobilization of FAM-NeoNectin^{E44C}. Cells within an unpatterned region are shown above and cells in a region photopatterned with immobilized protein are below. Scale bar = 50 μm. Individual cell measurements ($n = 250$ for each condition) are plotted over bars representing the mean ± SD. (E) Quantification of 3D cell eccentricity within NeoNectin-patterned and unpatterned regions. Student's *t*-test. *** = $p < 0.001$. (F) A representative cell from the protein-tethered region shows clear spreading and skeletal fiber formation. Scale bar = 25 μm.

NeoNectin^{E44C}. Additionally, 3D-encapsulated cells showed increasing eccentricity with pronounced protrusions as they interacted with tethered NeoNectin, while cells in unpatterned regions remained largely spherical (Figures 5C–F and S12). To the best of our knowledge, this represents the first use of a photopatterned *de novo*-designed protein to guide cell fate.

4 | Discussion

In this manuscript, we demonstrated that an inexpensive LCD printer can be repurposed for non-binary material fabrication/modulation, enabling rapid and high-fidelity encoding of grayscale input image templates into gel stiffness and biochemical cue presentation. This initial demonstration made use of a commercial LCD printer that could programmably emit low-intensity 405 nm light for photocustomization. While this low intensity is useful for the printer's originally intended application in layer-by-layer printing, the "thickness" of grayscale-patterned materials that can be readily processed is theoretically limited by absorption and scattering that can vary widely by application. For example, dense 3D cell assemblies (e.g., organoids) and naturally derived fibrous scaffolds (e.g., collagen, fibrin) can almost certainly be patterned on an LCD screen, but they will present different resolution and z-depth limits than optically clear, homogeneous step-growth hydrogels. In some of these cases, a printer equipped with a brighter LCD screen or an SLA printer with improved collimation may be more appropriate at a slightly higher cost. Similarly, printers with larger LCD screens are available if bigger patterned areas are needed. Either of these solutions remains cost-efficient and accessible to teams without extensive patterning experience.

In addition to thickness limitations potentially imposed by the printer's weak light source, the current LCD emission wavelength (405 nm) must be matched with chemistries that respond in a dose-dependent manner to visible light. Though there are many cytocompatible photochemistries that respond in this manner, many others require higher energy photons (e.g., 365 nm) for activation [36]. An LCD screen engineered to emit at these lower wavelengths, but in an otherwise similarly programmable manner, would substantially widen the library of chemistries that could be implemented and indeed already exist on the commercial market. Alternatively, the requirement to utilize visible light may help spur further innovation in the chemistry space [37, 38], further expanding the palette of red-shifted and dose-dependent photoreactions.

The method presented here is limited to 2D collimated patterns and is unable to include fully 3D features such as overhanging structures and voids. If desired, however, one could also imagine intentionally engineering an LCD-based printer for the purpose of grayscale 3D material photopolymerization. Grayscale DLP-based approaches (g-DLP) have begun to emerge in additive manufacturing research but have yet to gain traction in biomaterials fabrication [39]. Gradient SLA printing is generally challenging because light sources are ultimately binary and must be tuned after emission either by the photomask itself or through another workaround strategy. Conversely, laser lithography allows dynamic intensity switching in a pixel-by-pixel manner, but fabrication time scales linearly with construct size. Some recent studies have sought to circumvent the need for gradient light exposure altogether, opting for multiwavelength [40] or vat-switching [11, 41] strategies. In the case of LCD printing, a simple software update (e.g., adding a grayscale "mode" that allows multiple virtual layers to exist within each z slice) alongside reintroduction of the moving build stage could yield an inexpensive and effective solution for fabricating 3D objects with internally variable and non-binary stiffnesses. Truly grayscale LCD screens do exist, but they are uncommon and often only allow a limited range of simultaneous intensity values [42].

Finally, while this work has focused on controlling local reaction extent using purely synthetic chemistry-based reactions, we note that the overall approach could be similarly employed for optogenetic regulation of (intra)cellular processes. Given that many optogenetic systems respond to visible light, we would expect that porting this method to more "inside-out"-based approaches to be very straightforward. As more image-guided patterning strategies emerge, it will also be vital to match them with both "inside-out" and "outside-in" biological systems possessing complementary throughput–resolution requirements [43]. For example, extremely high resolution/low throughput laser fabrication techniques are well suited for addressing individual cells ($< 10\,\mu m$) or for spatiotemporal tuning of micron-scale processes such as organoid assembly [44]. Conversely, LCD patterning has extremely high volumetric throughput limited only by screen dimensions and can address biological chemical and mechanical gradients over distances as small as ~100 μm, ideal for modeling larger structures such as biological interfaces and whole tumors. We began exploring opportunities in this space by mimicking the SOX10 gene expression pattern from a murine melanoma with high spatial control. Given the wealth of existing high resolution biological image datasets and emerging gradient biofabrication technologies, there are endless opportunities to begin probing the complex relationship between geometry and function in living tissue.

5 | Conclusion

Though recent advancements in additive manufacturing have enabled hydrogels to be printed in user-defined geometries, techniques to variably specify graded physicochemical properties throughout this important class of biomaterials have been largely elusive. In this work, we established that light dose-dependent reactions can be employed alongside an inexpensive and minimally modified LCD printer to achieve grayscale image-guided patterning of hydrogel film stiffness and biochemistry. Showcasing the method's compatibility with many common biomaterial photochemistries, we spatially patterned the extent of polymerization of PEGDA-based gels, immobilization of biochemical cues via a photomediated oxime ligation, and 3D spreading of encapsulated mammalian cells in response to a *de novo*-designed protein tethered using a thiol-ene click reaction. While our initial motivation centered around the creation of patterned biomaterials to be used to study cell response to variable matrix-presented cues, we anticipate that fabrication approaches presented—particularly given their ease of implementation—will be of broad interest to other sectors of advanced manufacturing.

Acknowledgments

We thank the W.M. Keck Microscopy Center and Dr. Nathaniel Peters for training and assistance and for the use of their confocal microscope for FRAP imaging, as well as Murial Ross for providing the GFP for FRAP studies. This work was supported by a Faculty Early Career Development CAREER Award (DMR 1652141, C.A.D.) from the National Science Foundation (NSF) and a seed grant through the NSF-sponsored University of Washington Materials Research Science and Engineering Center (DMR 1719797 to C.A.D.), as well as a Maximizing Investigators' Research Award (R35GM138036 to C.A.D.) and a research grant (R01CA289291 to C.A.D.) from the National Institutes of Health. Graduate student fellowship support was provided by the ITHS (to R.M.F.) and an Interdisciplinary Training Grant (T32CA080416 to I.K.) from the National Institutes of Health. Additional funding was provided by the Howard Hughes Medical Institute (D.B.) and the Audacious Project (D.B., X.W.).

Conflicts of Interest

The authors declare no conflicts of interest.

Data Availability Statement

All pertinent experimental procedures, materials, methods, and characterization data are available within this manuscript and its associated Supporting Information.

References

1. C. A. DeForest and K. S. Anseth, "Advances in Bioactive Hydrogels to Probe and Direct Cell Fate," *Annual Review of Chemical and Biomolecular Engineering* 3 (2012): 421–444.

2. R. Gharios, R. M. Francis, and C. A. DeForest, "Chemical and Biological Engineering Strategies to Make and Modify Next-Generation Hydrogel Biomaterials," *Matter* 6 (2023): 4195–4244.

3. J. Lou and D. J. Mooney, "Chemical Strategies to Engineer Hydrogels for Cell Culture," *Nature Reviews Chemistry* 6 (2022): 726–744.

4. T. H. Qazi, M. R. Blatchley, M. D. Davidson, et al., "Programming Hydrogels to Probe Spatiotemporal Cell Biology," *Cell Stem Cell* 29 (2022): 678–691.

5. B. Grigoryan, S. J. Paulsen, D. C. Corbett, et al., "Multivascular Networks and Functional Intravascular Topologies Within Biocompatible Hydrogels," *Science* 364 (2019): 458–464.

6. P. N. Bernal, P. Delrot, D. Loterie, et al., "Volumetric Bioprinting of Complex Living-Tissue Constructs Within Seconds," *Advanced Materials* 31 (2019): 1904209.

7. T. J. Hinton, Q. Jallerat, R. N. Palchesko, et al., "Three-Dimensional Printing of Complex Biological Structures by Freeform Reversible Embedding of Suspended Hydrogels," *Science Advances* 1 (2015): e1500758.

8. L. L. Wang, C. B. Highley, Y. Yeh, J. H. Galarraga, S. Uman, and J. A. Burdick, "Three-Dimensional Extrusion Bioprinting of Single- and Double-Network Hydrogels Containing Dynamic Covalent Crosslinks," *Journal of Biomedical Materials Research Part A* 106 (2018): 865–875.

9. H. Liu, P. Chansoria, P. Delrot, et al., "Filamented Light (FLight) Biofabrication of Highly Aligned Tissue-Engineered Constructs," *Advanced Materials* 34 (2022): 2204301.

10. U. N. Lee, J. H. Day, A. J. Haack, et al., "Layer-By-Layer Fabrication of 3D Hydrogel Structures Using Open Microfluidics," *Lab on a Chip* 20 (2020): 525–536.

11. Q. Ge, A. H. Sakhaei, H. Lee, C. K. Dunn, N. X. Fang, and M. L. Dunn, "Multimaterial 4D Printing With Tailorable Shape Memory Polymers," *Scientific Reports* 6 (2016): 31110.

12. A. P. Dhand, M. D. Davidson, and J. A. Burdick, "Lithography-Based 3D Printing of Hydrogels," *Nature Reviews Bioengineering* 3, no. 2 (2024): 108–125, https://doi.org/10.1038/s44222-024-00251-9.

13. C. Li, L. Ouyang, J. P. K. Armstrong, and M. M. Stevens, "Advances in the Fabrication of Biomaterials for Gradient Tissue Engineering," *Trends in Biotechnology* 39 (2021): 150–164.

14. E. R. Ruskowitz and C. A. DeForest, "Photoresponsive Biomaterials for Targeted Drug Delivery and 4D Cell Culture," *Nature Reviews Materials* 3 (2018): 17087.

15. R. M. Francis and C. A. DeForest, "4D Biochemical Photocustomization of Hydrogel Scaffolds for Biomimetic Tissue Engineering," *Accounts of Materials Research* 4 (2023): 704–715.

16. I. Kopyeva, R. P. Brady, and C. A. DeForest, "Light-Based Fabrication and 4D Customization of Hydrogel Biomaterials," *Nature Reviews Bioengineering* 3, no. 2 (2024): 159–180, https://doi.org/10.1038/s44222-024-00234-w.

17. S. C. P. Norris, P. Tseng, and A. M. Kasko, "Direct Gradient Photolithography of Photodegradable Hydrogels With Patterned Stiffness Control With Submicrometer Resolution," *ACS Biomaterials Science & Engineering* 2 (2016): 1309–1318.

18. G. I. Peterson, J. J. Schwartz, D. Zhang, et al., "Production of Materials With Spatially-Controlled Cross-Link Density via Vat Photopolymerization," *ACS Applied Materials & Interfaces* 8 (2016): 29037–29043.

19. I. Batalov, J. R. Filteau, R. M. Francis, et al., "Grayscale 4D Biomaterial Customization at High Resolution and Scale" (2024), https://doi.org/10.1101/2024.01.31.578280.

20. Z. Zhao, J. Wu, X. Mu, H. Chen, H. J. Qi, and D. Fang, "Origami by Frontal Photopolymerization," *Science Advances* 3, no. 4 (2017): e1602326, https://doi.org/10.1126/sciadv.1602326.

21. V. Karamzadeh, M. L. Shen, H. Ravanbakhsh, et al., "High-Resolution Additive Manufacturing of a Biodegradable Elastomer With A Low-Cost LCD 3D Printer," *Advanced Healthcare Materials* 13 (2024): 2303708.

22. D. M. Soumpasis, "Theoretical Analysis of Fluorescence Photobleaching Recovery Experiments," *Biophysical Journal* 41 (1983): 95–97.

23. N. R. Richbourg and N. A. Peppas, "High-Throughput FRAP Analysis of Solute Diffusion in Hydrogels," *Macromolecules* 54 (2021): 10477–10486.

24. K. S. Lim, B. J. Klotz, G. C. J. Lindberg, et al., "Visible Light Cross-Linking of Gelatin Hydrogels Offers an Enhanced Cell Microenvironment With Improved Light Penetration Depth," *Macromolecular Bioscience* 19 (2019): 1900098.

25. I. Batalov, K. R. Stevens, and C. A. DeForest, "Photopatterned Biomolecule Immobilization to Guide Three-Dimensional Cell Fate in Natural Protein-Based Hydrogels," *Proceedings of the National Academy of Sciences* 118 (2021): e2014194118.

26. D. R. Stirling, M. J. Swain-Bowden, A. M. Lucas, A. E. Carpenter, B. A. Cimini, and A. Goodman, "CellProfiler 4: Improvements in Speed, Utility and Usability," *BMC Bioinformatics* 22 (2021): 433.

27. B. D. Fairbanks, M. P. Schwartz, C. N. Bowman, and K. S. Anseth, "Photoinitiated Polymerization of PEG-Diacrylate With Lithium Phenyl-2,4,6-Trimethylbenzoylphosphinate: Polymerization Rate and Cytocompatibility," *Biomaterials* 30 (2009): 6702–6707.

28. V. Hagen, B. Dekowski, V. Nache, et al., "Coumarinylmethyl Esters for Ultrafast Release of High Concentrations of Cyclic Nucleotides Upon One- and Two-Photon Photolysis," *Angewandte Chemie, International Edition* 44 (2005): 7887–7891.

29. N. Broguiere, I. Lüchtefeld, L. Trachsel, et al., "Morphogenesis Guided by 3D Patterning of Growth Factors in Biological Matrices," *Advanced Materials* 32 (2020): 1908299.

30. I. Kopyeva, E. C. Goldner, J. W. Hoye, et al., "Stepwise Stiffening/Softening of and Cell Recovery From Reversibly Formulated Hydrogel

Interpenetrating Networks," *Advanced Materials* 36, no. 44 (2024): 2404880, https://doi.org/10.1002/adma.202404880.

31. P. Crisalli and E. T. Kool, "Water-Soluble Organocatalysts for Hydrazone and Oxime Formation," *Journal of Organic Chemistry* 78 (2013): 1184–1189.

32. A. Blaeser, D. F. Duarte Campos, and H. Fischer, "3D Bioprinting of Cell-Laden Hydrogels for Advanced Tissue Engineering," *Current Opinion in Biomedical Engineering* 2 (2017): 58–66.

33. X. Zhang, S. M. Pant, C. C. Ritch, et al., "Cell State Dependent Effects of Bmal1 on Melanoma Immunity and Tumorigenicity," *Nature Communications* 15 (2024): 633.

34. X. Wang, J. Guillem-Marti, S. Kumar, et al., De Novo Design of Integrin α5β1 Modulating Proteins for Regenerative Medicine (2024), https://doi.org/10.1101/2024.06.21.600123.

35. J. A. Shadish and C. A. DeForest, "Site-Selective Protein Modification: From Functionalized Proteins to Functional Biomaterials," *Matter* 2 (2020): 50–77.

36. P. Klán, T. Šolomek, C. G. Bochet, et al., "Photoremovable Protecting Groups in Chemistry and Biology: Reaction Mechanisms and Efficacy," *Chemical Reviews* 113 (2013): 119–191.

37. T. L. Rapp and C. A. DeForest, "Visible Light-Responsive Dynamic Biomaterials: Going Deeper and Triggering More," *Advanced Healthcare Materials* 9 (2020): 1901553.

38. T. L. Rapp and C. A. DeForest, "Tricolor Visible Wavelength-Selective Photodegradable Hydrogel Biomaterials," *Nature Communications* 14 (2023): 5250.

39. X. Kuang, J. Wu, K. Chen, et al., "Grayscale Digital Light Processing 3D Printing for Highly Functionally Graded Materials," *Science Advances* 5 (2019): eaav5790.

40. L. Yue, S. Macrae Montgomery, X. Sun, et al., "Single-Vat Single-Cure Grayscale Digital Light Processing 3D Printing of Materials With Large Property Difference and High Stretchability," *Nature Communications* 14 (2023): 1251.

41. Q. Ge, Z. Chen, J. Cheng, et al., "3D Printing of Highly Stretchable Hydrogel With Diverse UV Curable Polymers," *Science Advances* 7, no. 2 (2021): eaba4261, https://doi.org/10.1126/sciadv.aba4261.

42. T. Hayashi, T. Shibata, T. Kawashima, E. Makino, T. Mineta, and T. Masuzawa, "Photolithography System With Liquid Crystal Display as Active Gray-Tone Mask for 3D Structuring of Photoresist," *Sensors and Actuators A: Physical* 144 (2008): 381–388.

43. C. A. DeForest, B. E. Kirkpatrick, and K. S. Anseth, "Engineering Native Biological Complexity From the Inside–Out and Outside–in," *Nature Chemical Engineering* 1 (2024): 2–5.

44. N. Gjorevski, M. Nikolaev, T. E. Brown, et al., "Tissue Geometry Drives Deterministic Organoid Patterning," *Science* 375, no. 6576 (2022): eaaw9021, https://doi.org/10.1126/science.aaw9021.

Supporting Information

Additional supporting information can be found online in the Supporting Information section.